

BERP: A Blind Estimator of Room Acoustic and Physical Parameters for Single-Channel Noisy Speech Signals

Lijun Wang ^{*} *Graduate Student Member, IEEE*, Yixian Lu ^{*}, Ziyan Gao *Member, IEEE*, Kai Li, Jianqiang Huang, Yuntao Kong, and Shogo Okada *Member, IEEE*

arXiv:2405.04476v5 [eess.AS] 24 Oct 2024

Abstract—Room acoustic parameters (RAPs) and room physical parameters (RPPs) are essential metrics for parameterizing the room acoustical characteristics (RACs) of a sound field around a listener’s local environment, offering comprehensive indications for various applications. Current RAP and RPP estimation methods either fall short of covering broad real-world acoustic environments in the context of real background noise or lack universal frameworks for blindly estimating RAPs and RPPs from noisy single-channel speech signals, particularly sound source distances, direction of arrival (DOA) of sound sources, and occupancy levels. On the other hand, in this paper, we propose a new universal blind estimation framework called the blind estimator of the room acoustical and physical parameters (BERP), by introducing a new stochastic room impulse response (RIR) model, namely the sparse stochastic impulse response (SSIR) model, and endowing the BERP with a unified encoder and multiple separate predictors to estimate RPPs and SSIR parameters in parallel. This estimation framework enables computationally efficient and universal estimation of room parameters using solely noisy single-channel speech signals. Finally, all RAPs can be simultaneously derived from RIRs synthesized from the SSIR model with estimated parameters. To evaluate the effectiveness of the proposed BERP and SSIR models, we compile a task-specific dataset from several publicly available datasets. The results reveal that the BERP achieves state-of-the-art (SOTA) performance. In addition, the evaluation results for the SSIR RIR model also demonstrated its efficacy. The code is available on GitHub.¹

Index Terms—Room acoustics, Room impulse response, Blind estimation, Reverberation time, Room acoustic parameters, Attention mechanism

I. INTRODUCTION

ROOM acoustical characteristics (RACs) characterize the room acoustical properties through which people perceive the sound in an enclosure. RACs determine how intelligibly and clearly people perceive sound in an auditory space encompassed by the walls, ceilings, and furniture. For example, concert halls require clear and transparent sounds for music appreciation, whereas lecture rooms seek intelligible delivery for lectures and public addresses. General auditoriums require intelligible and easily audible sounds [1]. Local RACs,

L. Wang, Y. Lu, Z. Gao, K. Li, J. Huang, Y. Kong, and S. Okada are with School of Information Science, Japan Advanced Institute of Science and Technology, Ishikawa, Japan. email: {lijun.wang, ziyan-g, kai-li, jq.huang, okada-s, yuntao.kong}@jaist.ac.jp (*Corresponding author: okada-s@jaist.ac.jp*)

Y. Lu is with ACES, Inc., Tokyo, Japan. email: mcluoc@gmail.com

This work was partially supported by the Japan Society for the Promotion of Science (JSPS) KAKENHI (grant numbers 23H03506).

^{*}Equal Contribution.

1 The code and weights are available at <https://github.com/Alized/BERP>.

which refer to the RACs perceived within the listener’s local surroundings, are widely employed in speech enhancement, hearing aids, immersive audio, context-aware renderings (such as mixed reality and augmented reality), public address systems, and robotic systems. Compared to global RACs that reflect the stationary attributes of room acoustics, the dynamic parameterization of local RACs poses a significant challenge in room acoustics, given the interference caused by background environmental noise.

While a room impulse response (RIR) can fully represent a listener’s local RACs, it does not provide a direct interpretation of how the human perceives their local RACs, i.e., the subjective perception of the local RACs. Since speech intelligibility and sound clarity are subjective perceptions, subjective listening experiments are typically conducted to assess them. Alternatively, the objective indices [2] (i.e., RAPs) can be measured in situ to assess speech intelligibility and sound clarity from the measured RIR. However, on the one hand, conducting listening experiments is expensive and time-consuming, making them impractical to apply in public spaces [3]. On the other hand, measuring RIR is not always feasible in all scenarios, which we discuss in the next paragraph. Additionally, physical geometry-related information, such as room volumes, distances from sound sources, and the corresponding orientations, which have critical applications in spatial audio rendering, intelligibility assessments in a room, separation of sound sources, audio navigation system, and speech enhancement [4]–[10], is lacking. Consequently, room acoustic parameters (RAPs) and room physical parameters (RPPs) have been used to model local RACs to offer clear and comprehensive indications for various applications, such as room acoustical assessment [2], [8], [11]–[13], speech enhancement [10], [14], [15], hearing aids [7], [16]–[20], sound source separation [4], [5], spatial audio rendering [21], context-aware rendering in extended reality (XR) and augmented reality (AR) [6], [22], [23], public address systems [24], [25], and robotics [26]. Here, the adjective “physical” means room-geometrical related. In this paper, physical and geometric are interchangeable.

A few RAPs have been investigated and standardized [2], [11], [12], [27]. In IEC60268-16:2020, the speech transmission index (STI) is used to predict the speech intelligibility of an enclosure. The percentage articulation loss of consonants (%AL_{cons}) [12] was studied to compensate for the limitations of STI, which has difficulty in reflecting the effect of linguistic

information on perception of intelligibility. The essential RAPs and their corresponding measurements, including reverberation time (T_{60}), early decay time (EDT), clarity (C_{80} / C_{50}), definition (D_{50}), and center time (T_s), have been standardized in ISO 3382-1:2009 [2]. T_{60} is the most essential RAP for representing the RACs of an enclosure. RAPs can be directly derived from the measured RIR. The measurement of RIR requires the exclusion of all people located in an enclosure, which is impractical for public spaces, as the measurement of RIR requires high-energy sound [28], [29]. Furthermore, the RIR measurement is limited to capture the dynamics of the local RACs, which vary according to the locations, arrangements, and quantities of the objects and occupants that are present. The RAPs measured using specific standards may differ from non-compliant measurements employed within the same enclosure. Therefore, a blind RAP estimation method is imperative, particularly in public spaces where people cannot be excluded. Several RPPs have been studied [6], [7], [27], [30], [31], such as the room volume, the sound source distance, and direction-of-arrival (DOA) of the sound source. The room volume is closely related to the RACs [6], [7], [27]. It may be derived from the measured RIR, but this process encounters the aforementioned issues. Moreover, the sound source distance and DOA are observer-dependent parameters. Thereby, blind estimation methods have been proposed to obtain the RAPs and RPPs from the observed signals. Blind estimation is a challenging task, since it is an ill-posed problem that derives a system solely from an output without prior knowledge of the input.

Deep learning techniques are well suited to construct complex mappings between high-dimensional data acquired from messy realistic environments, often without explicit indications of relevance [32]. Hence, the common approach of blind estimation is to establish a mapping from the observed signals to the output using deep learning techniques.

In terms of blind RAP estimation in scenarios with background noise, deep learning techniques are currently at the forefront of this field. Several methods utilizing fully convolutional neural networks (CNN) have achieved blind reverberation time and room volume estimation from Gammatonegrams of single-channel noisy speech signals [33], [34] leveraging the network architecture originally developed by Gamper and Tashev [35]. Furthermore, López et al. [36] and Callens et al. [37] introduced the convolutional recurrent neural networks (CRNN) architecture, which outperformed the best model in the ACE challenge [38], for universally estimating the reverberation time, clarity, and direct-to-reverberation ratio from the mel frequency cepstral coefficients (MFCC) of single-channel noisy speeches. Zheng et al. [39] proposed a CNN method with a gating mechanism that was designed to estimate the reverberation time in noisy conditions using the spectrogram of the observed signal. Duangpummet et al. [29] developed a TAE-CNN architecture using the temporal amplitude envelope (TAE) of the observed signal, allowing concurrent estimation of STI, reverberation time, clarity, definition, and center time. For blind estimation of RPPs, a fully CNN architecture was employed to estimate room volumes from single-channel speech signals in [33], [34]. Furthermore, the

CRNN architecture was deployed to estimate sound source distances and the DOAs of sound sources from multichannel speech signals [30]. Neri [40] combined the gated recurrent unit (GRU) and CNN to blindly estimate the sound source distance from single-channel speech signals.

Several previous methods have imposed constraints in terms of insufficient coverage of RIRs to accommodate real-world scenarios to the greatest extent possible. For example, in [29], [36], [37], they restricted the range of RIRs in which the reverberation time T_{60} ranges from 0.2 to 2.5 s. Studies by [35] and [39] have also limited T_{60} to 1.5 s.

On the other hand, the current methods rely on the synthetic RIRs to synthesize the observed reverberant signals to train the model. These synthetic RIR algorithms include adaptive rectangular decomposition (ARD) using finite-difference time-domain (FDTD) [41] as employed in [34], algorithms based on source image model such as pyroomacoustic [42] used in [33] and RIR generator [43] used in [39], and stochastic extended RIR model used in [29]. The limitations of synthetic RIRs are presented as follows. First, RIR simulation algorithms [42], [43] employed in [33] and [39] do not adequately account for complex real-world room geometries with intricate decorated materials, complex-shaped decorations, furniture and objects, such as the irregular-shaped concert halls with delicate decorations and infrastructures that balances the functionality and aesthetics, although source image principle used in these RIR simulation algorithms is suitable for modeling room acoustics in rooms with arbitrary room geometries [44]. As noted in [45], the limitation of RIR simulation algorithms based on source image does not stem from the source image principle itself, but rather from the simplification of room geometries and materials. This simplification typically involves reducing the complexity of details such as the absorption and scattering coefficients of the room surfaces and complex wave phenomena due to the complicated room geometries, as also noted in [33]. The coefficients and wave phenomena are greatly influenced by the furniture, objects, and wall materials in real rooms [46], [47]. Besides, the synthetic RIRs using ARD with FDTD [41] used in [34] lack some expected irregularity features of realistic RIRs, as also indicated by [34], causing the risk of overfitting if the dataset is largely synthetic [48]. [29] employed a stochastic RIR model to generate synthetic RIRs and synthesized the observed signals using the synthetic RIRs solely. Nevertheless, the stochastic RIR model they used is not appropriate as it contradicts the sparse statistical property of the early reflection in realistic RIRs [44], [49], since they modeled the early reflection of RIR as a centered Gaussian process. Therefore, we intend to use realistic RIRs exclusively to synthesize the observed signals to maximally reflect the real-world acoustical environments and mitigate the risk of overfitting, as well as reducing the sim-to-real gap.

Besides the aforementioned issues, another challenge is to train a universal architecture that is capable of simultaneously and efficiently estimating RAPs and RPPs in a unified methodology, especially for instantaneous occupancy levels. To the best of our knowledge, no learning-based schemes are available for the blind estimation of the DOAs of sound sources from single-channel speech signals. The difficulty

of extracting positional information from the single-channel signals lies in the usage of single spectral cues alone, unlike multi-channel signals where spatial cues between channels can be used. Additionally, since single-channel spectral cues have been reported to be used to estimate DOAs [50], [51], it is possible to estimate sound source distances from the same cues using deep learning techniques.

These gaps motivate us to propose a new method, a blind estimator of room acoustic and physical parameters (BERP), that can blindly estimate room parameters universally in various real-world acoustic environments with background environmental noise. We integrate a sparse stochastic impulse response (SSIR) model, a new stochastic RIR model, into the process of mapping the desired RAPs and the observed speech signals. This RIR model fuses the distinct statistical properties, i.e., the sparse and dense statistical properties of different segments of realistic RIRs, to model realistic RIRs more accurately. The SSIR model can help to simultaneously derive all RAPs without introducing additional complexity to the trainable model by establishing only the mapping between the parameters of the SSIR and the observed signals. In contrast, we directly establish the relationship between the RPPs and the observed signals by using neural networks. Presently, except for the occupancy level, BERP assumes a single-source speech signal of dynamic movement as the observed input. This assumption, while effective for many scenarios, may not fully capture the complexity of real-world acoustic environments. More detailed discussions of current limitations and future work are included in Sec. V.

Our work makes three important contributions to the temporary knowledge frontier, as follows:

- A new stochastic RIR model is proposed to effectively model the realistic RIRs in terms of simultaneous RAP derivations.
- Signal models for estimating observed speech signals at the listener's local, especially the occupancy level estimation, and corresponding data synthesis pipelines are proposed.
- A new universal blind estimation framework for blindly estimating RAPs and RPPs in parallel is proposed, which achieves state-of-the-art (SOTA) performance.

The rest of the paper is composed as follows. Section II briefs RAPs and RPPs. The proposed method is introduced in Section III and the corresponding experimental settings are outlined in Section IV. We discuss and conclude in Section V.

II. ROOM PARAMETERS

A. Room Acoustic Parameters

Several RAPs that describe RACs of an auditory space have been investigated and standardized [2], [11], [27], [45], [52]–[54]. The parameters that are widely used to parameterize room acoustics by audio engineers are briefly introduced.

1) *Intelligibility Parameters*: Intelligibility parameters, including STI and $\%AL_{cons}$, are used to predict speech intelligibility and assess verbal comprehension in a sound field.

Speech intelligibility index. The STI is employed to predict speech intelligibility and the corresponding listening difficulty

in noisy surroundings. Houtgast and Steeneken initially defined the STI based on the modulation transfer function (MTF) [55], [56]. The higher the STI, the more intelligible the sound field. STI can be calculated from the RIR as follows, which was standardized by IEC 60286-16:2020 [11].

Percentage articulation loss of consonants. $\%AL_{cons}$ accounts for the measurement of incorrectly understood consonants, and this measure was originally introduced by Peutz and Kelin [12]. Since the STI does not account for the way in which a listener's proficiency and linguistic knowledge affect the intelligibility, $\%A_{cons}$ assumes that consonants are harder to comprehend than vowels in a room. The utility of $\%A_{cons}$ extends the limitations of the STI by not discounting significant information related to intelligibility and considering linguistic proficiency. Moreover, its robustness against guessing contamination makes it a great indicator of speech intelligibility [7]. Thus, $\%AL_{cons}$ emerges as an indispensable complement to the STI to comprehensively evaluate speech intelligibility in various room settings. $\%AL_{cons}$ can be steadily calculated from the STI according to Farrell Becker's empirical formula [57]:

$$\%AL_{cons} = 170.5045 \cdot e^{-5.419 \cdot STI}. \quad (1)$$

2) *Reverberation Parameters*: Reverberation time (T_{60}) and early decay time (EDT) are relevant to reverberation and quantify the subjective impression of the vivacity of a sound field. T_{60} is the most essential RAP, as it characterizes the physical properties of the RACs for which the reverberation energy is distributed within -60 dB. The EDT represents the decay time for the initial 10 dB to emphasize the more important contribution of early reflection to perceived reverberation. Both RAPs are derived from the RIR using Schroeder's back integration method [58]. We adhere to ISO 3382-1:2009 standard [2] for calculating T_{60} and EDT, consistent with the approach used in several baseline methods [29], [33], [35]–[37]. T_{60} is the 60-dB decay time calculated by line-fitting to the proportion of the energy decay curve (EDC) of the RIR from -5 dB to -35 dB and linearly extrapolating it to -60 dB. Similarly, the EDT is to line-fit the initial -10 dB of the EDC and to extrapolate to -60 dB.

3) *Energy Parameters*: Clarity (C_{50} and C_{80}), definition (D_{50}), and center time (T_s) are the energy parameters used to measure the energy ratio of the RIR between the energy contributed from early reflections and late reverberation. They are strongly related to the impression of transparency. The calculation methods for these four RAPs have been standardized in ISO 3382-1:2009 [2]. We use the calculation methods defined in the standard.

Clarity. C_{80} and C_{50} express the logarithmic ratio of the energy within the first 50 ms for speech and that within the first 80 ms for music to the remaining RIR, thus characterizing the clarity perception of a speech or music signal traversing within a room [59], [60]. Clarity can be defined as:

$$C_{t_e} = 10 \log_{10} \left(\frac{\int_0^{t_e} h^2(t) dt}{\int_{t_e}^{\infty} h^2(t) dt} \right) \quad (2)$$

where t_e denotes 50 or 80 ms, respectively.

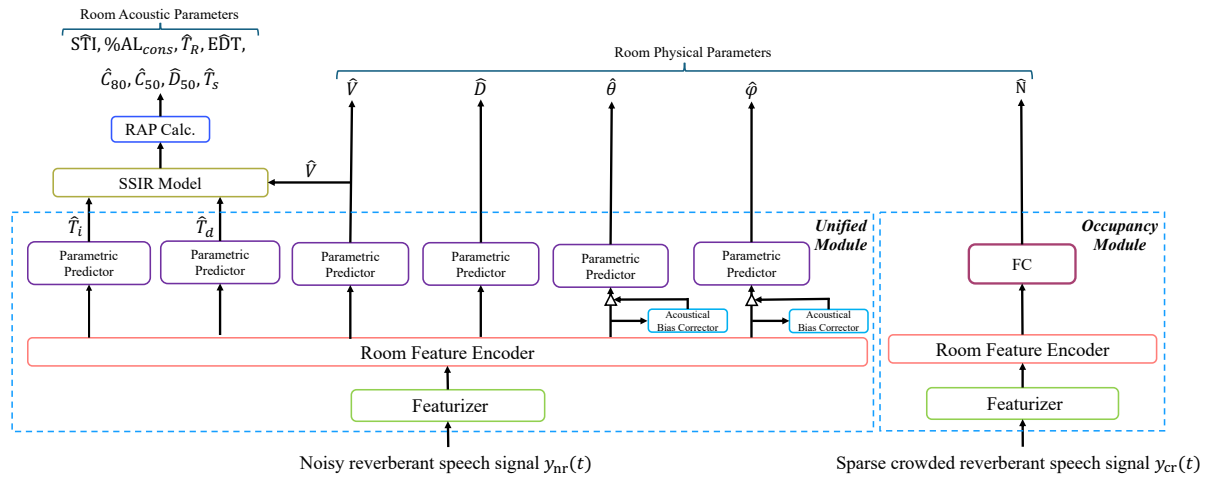


Fig. 1: Overview of the architecture of the blind estimator of room acoustic and physical parameters (BERP). The input includes the observed speech signals within a room, which are the observed noisy and crowded reverberant speech signals, while the output contains the estimated RAPs and RPPs detailed in Section II-A and II-B, respectively. The architecture can adapt to various input lengths without the need for length alignment. Fig. 6-8 shows the detailed architectures of the room feature encoder, Fig. 9 corresponds for the parametric predictor, and Fig. 11 is the architecture of the acoustical bias corrector.

Definition. D_{50} indicates the subjective intelligibility of speech in a room, which is defined as the ratio of the energy received within 50 ms to the total energy of the RIR [61].

$$D_{50} = \frac{\int_0^{50 \text{ ms}} h^2(t) dt}{\int_0^{\infty} h^2(t) dt} \times 100. \quad (3)$$

Center time. T_s refers to ‘‘the center of gravity time’’, characterizing the balance between clarity and reverberation that is related to speech intelligibility [62]. T_s is given by:

$$T_s = \frac{\int_0^{\infty} t h^2(t) dt}{\int_0^{\infty} h^2(t) dt}. \quad (4)$$

B. Room Physical Parameters

RPPs are parameters related to the physical characteristics of a room. These parameters encompass the geometric room volume, sound source distance, DOA of the sound source, and the instantaneous occupancy level around the listener’s location.

1) *Geometric Room Volume*: The geometric room volume V is a position-independent parameter to model the attributes of a room. V is strongly related to the estimation of *critical distance* (D_c), which is the distance from the sound source at which the energy density of the reverberant signal is equal to that of the direct signal [27]. D_c can be approximated using Sabine’s formula:

$$D_c = \sqrt{\frac{\varrho A}{16\pi}} \approx 0.1 \sqrt{\frac{\varrho V}{\pi T_{60}}} \quad (5)$$

where ϱ signifies the source directivity factor, and A represents the equivalent absorption area of a room. D_c is vital for determining whether a virtual sound source should be rendered with reverberation, thus serving as a key distance cue for the perception of reverberation by the listener [27], [34].

Furthermore, the mixing time used in AR rendering applications [6] can be determined from V as $t_m = \sqrt{V}$. Jot et al. [6] identified room volume as a reverberation fingerprint to characterize rooms for spatial AR rendering. V also plays

an important role in speech intelligibility [7]. The *critical distance of intelligibility* (D_{ci}), which acts as a distance cue for perceived intelligibility, is derived from V as:

$$D_{ci} = 0.2 \sqrt{\frac{\varrho V}{T_{60}}}. \quad (6)$$

$\%AL_{cons}$ also exhibits a strong relationship with V , which can be alternatively expressed as [7]:

$$\%AL_{cons} = \frac{200 D^2 T_{60}^2}{\varrho V} + c. \quad (7)$$

D is the sound source distance, and c is the correction factor.

2) *Sound Source Distance*: The sound source distance D contributes significantly to complementing the sound source localization (SSL) by integrating it with the DOA of the sound source [30]. SSL is widely used in applications such as sound source separation [4], audio-oriented and navigational systems [9], speech-related applications [31], and human-robot interaction [26]. Furthermore, D is intimately related to the perception of speech intelligibility, particularly in terms of $\%AL_{cons}$, as elaborated in Eq. (7).

3) *Direction-of-Arrival of the Sound Source*: As mentioned in Section II-B2, the DOA is a crucial component of SSL [31], and it has several applications in sound source separation [5], speech recognition [20], speech enhancement [10], and room acoustical analysis [8]. In this work, the DOA is represented by a pair that includes an azimuth (θ) and elevation (ψ) and is denoted as $\text{DOA} := \{\theta, \psi\}$.

4) *Instantaneous Occupancy Level*: The detection of the instantaneous occupancy level of room N around a listener’s location is highly useful for several applications. It is commonly known that the number of occupants affects the reverberation [63], thus affecting the efficacy of demand-driven hearing aid systems and speech enhancement methods. In addition, interference speeches generated by the occupants around the listener affect the target signals that the listener intends to receive. Knowing the occupancy level helps control interference to achieve intelligible and clear transmission.

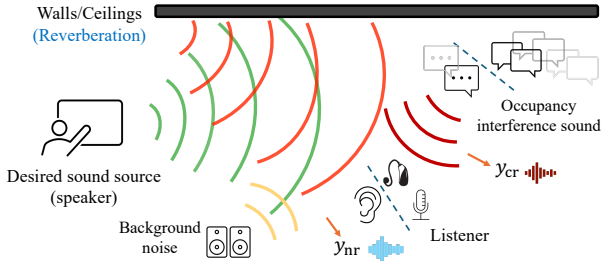


Fig. 2: Illustration of noisy and crowded reverberant signals y_{nr} and y_{cr} , respectively, in real-world scenarios.

In the context of smart homes, the estimated number of occupants can optimize the control of demand-driven heating, ventilation, and air conditioning (HVAC) operations in the local space to significantly reduce the cost of building operations for sustainable smart buildings [64], [65]. In the XR and AR scenarios, the local occupancy level, as an important factor in environmental information factor, is fundamental to ensuring safe interaction in real-world scenes, especially in public spaces populated by others.

III. PROPOSED METHOD

Overview: BERP. Fig. 1 shows the signal flow process within the proposed BERP framework. The input waveform is converted into a spectrogram-variant feature representation, which is subsequently fed into the room feature encoder (RFE). Finally, parametric predictors (PP) and a fully-connected (FC) layer output room parameters based on different estimation tasks for different real-world scenarios. When estimating RAPs and RPPs, except the occupancy level, noisy reverberant speech signals serve as the observed signal inputs for the featurizer. In contrast, when estimating the instantaneous occupancy level N , the crowded reverberant speech signals are the inputs of the featurizer.

A. Signal Models

1) *Noisy Reverberant Signal Model:* The observed noisy reverberant signal, as perceived by a listener while transmitting from a speaker within a room and subject to the influence of the background environmental noise, can be formulated as:

$$y_{nr}(t) = x(t) * h(t) + n(t) \quad (8)$$

where $y_{nr}(t)$ denotes the noisy reverberant signal as perceived by the listener, $h(t)$ denotes the RIR, and $n(t)$ represents the background noise that is prevalent in the listener's local surroundings. The symbol “ $*$ ” denotes the convolution operation.

The y_{nr} encapsulates the RIR information that fully characterizes the RACs in the listener's local space, including RAPs and room volume. In addition, it contains information pertaining to sound source localization, such as the distance, azimuth, and elevation. Therefore, this signal model is instrumental for parameterizing the listener's local acoustic space, encompassing aspects such as the volume, the distance and DOAs of the sound source, and RAPs. The noisy reverberant signal model is employed to model the real-world scenarios in which a listener interacts with a single speaker in the presence of environmental background noise, as illustrated in Fig. 2.

2) *Sparse Crowded Reverberant Signal Model:* Currently, the research domain lacks a comprehensive reverberant speech corpus for crowded environments that can enable the estimation of the occupancy level around the listener's local space, which encompasses complete meta-information, including the number of speakers, the spatial geometry of speaker distribution relative to the listener, and the local RACs where the listener occupies. We introduce a new signal model that incorporates this detailed meta-information to address this gap, as shown in Fig 2. This signal model can be expressed as:

$$y_{cr}(t) = \sum_{i=1}^N \left[\frac{d_0}{d_i} A_0 x_i(t) * h_i(t) \right] + n(t), \quad (9)$$

where y_{cr} signifies the crowded reverberant speech signal, $x_i(t)$ represents the speech signal originating from the i -th speaker proximal to the listener, and d_i denotes the distance between the i -th speaker and the listener, which adheres to a Gaussian distribution. A_0 represents the baseline amplitude observed at a distance of d_0 from the listener, i.e., the original amplitude of the speech $x_i(t)$ without attenuation. $h_i(t)$ denotes the processed RIR that retains only the reverberation-related acoustic characteristics of the local room while excluding positional-dependent information, as the positional-dependent information has already provided in the former term. $n(t)$ denotes the background noise.

As McKenzie et al. [66] demonstrated that direct sound carries the highest perceptual importance and positional information, which does not primarily reflect reverberation-related characteristics that vary much less with position, such as reverberation and spaciousness. Therefore, we filtered out the direct sound component (initially 4.17 ms [66]) of the RIR. Additionally, we normalize the amplitude of $h(t)$ unitarily to eliminate sound source distance cues related to the RIR amplitude. These steps discard position-dependent information to the largest extent feasible, ensuring that the RIR used in this signal model represents only reverberation-related acoustical characteristics. After that, the signal model can be simplified as:

$$y_{cr}(t) = \left[\sum_{i=1}^N \frac{d_0}{d_i} A_0 x_i(t) \right] * h(t) + n(t), \quad (10)$$

where d_0 is assumed to be equal to 1.0, which is the proper choice taking into account the preferred interpersonal distance [67]. The proposed model assumes that the distance from the i -th speaker to the listener should exceed d_0 , (i.e., it defines a minimal circular boundary around the speaker based on the preferred interpersonal distance [67]), and the amplitude corresponding to each occupant decays proportionally in accordance with the multiplicative inverse of the associated distance [64]. N represents the total count of speakers, i.e., the occupancy level, following the discretized Gamma distribution taking only integer values, which is detailed in Assumption 3.

When developing this speech signal model, a set of fundamental assumptions is postulated. These assumptions are instrumental for enabling an approximation that closely mirrors real-world scenarios while effectively reducing the complexities of the signal model.

Assumption 1. We hypothesize that the maximum spatial extent surrounding the listener is approximately 6 meters,

which speech signals from nearby occupants attenuate 22.6 over hard grounds and 24.8 dB over soft grounds.² Based on the normal speech sound pressure level (SPL) of about 69 dB at 1.0 m distance [70], rendering a speech beyond 6.0 m is approximately the same SPL (approximately 42 dB) in a quiet space, which is easily masked by background noise. Thus, occupant speech signals beyond the 6-meter threshold are viewed as background noise.

Assumption 2. The model assumes that the upper limit imposed on the number of speakers near the listener, i.e., N , is restricted to 12. Given that the area within a 6-meter radius is about 110.0 m^2 and considering a preferred social distance 1.4 m for a occupant [67] (resulting in an individual space of about 6.2 m^2 per person), the theoretical maximum occupancy without considering comfort or grouping is approximately 17 occupants. However, to account for more realistic daily life scenarios where maximum density is rarely achieved and to simplify our model, we set the maximum occupants to a sparser 12 occupants. On the other hand, setting this number results from considering the distinguishability of the overlapped speeches (i.e., too much overlap results in an indistinguishable speech signal), which is the precondition that blind estimation of the occupancy level can work. Although setting a maximum of 12 occupants also takes into account that heavily overlapping concurrent speech signals may blend into background noise that potentially reduces their individual discernibility, this consideration could be viewed as a plausible assumption to manage the complexity of the current model rather than a definitive scientific conclusion. More studies are needed to characterize this consideration across various acoustic conditions.

Assumption 3. This assumption determines the parameters of the discretized Gamma distribution that models the occupancy levels around the main listener (observer) as we mentioned earlier. We select the discretized Gamma distribution since it is well-suited for modeling positive integer-valued data and is often used to describe the time until a certain number of events occurs [71, Ch.5]. In our context, the occupancy level can be regarded as discrete independent events per unit time, as illustrated in Fig. 5. Next, the key challenge is to determine the shape and scale parameters of the discretized Gamma distribution. As it is hard to directly create a discretized Gamma distribution for practical implementation, we instead approximate it using a mixture of truncated Gaussian distributions that retains only positive values. In this Gaussian mixture model, only the shape parameter can be determined. To simplify the model and consider the sparse distribution of occupants (not too many occupants concentrate together in a small area of a public space), we heuristically assume that the most likely number of occupants a listener to engage with within a 6-meter radius area ranges from 3 to 4, i.e., the shape parameter of the discretized Gamma distribution.³

²The attenuation is calculated from <https://noisetools.net/barriercalculator>, according to ISO 9613-2:2024 [68] and ISO 9613-1:1993 [69].

³The corresponding approximation method for discretized Gamma distribution is detailed in data preprocessing pipeline https://github.com/Alizede/BERP/blob/main/notebooks/dataset_preprocess.ipynb.

3) Sparse Stochastic Impulse Response Model: Within the scope of dynamic blind RAPs and RPPs estimation, our access is restricted to an observed noisy reverberant signal. Hence, we model the observed signal as in Eq. (8). The ill-posed nature of blind estimation necessitates an RIR model to approximate an unknown RIR to serve as a bridge between the sound source signal and the perceived noisy reverberant signal.

Moreover, to reduce computational complexity and to facilitate their simultaneous estimation, it is more efficient to model the RIR and subsequently estimate the parameters of this RIR model. This approach enables the simultaneous derivation of the RAPs from the modeled RIR instead of directly estimating them from the noisy reverberant signal.

Generally, the RIR can be partitioned as the *early reflection* and *late reverberation*, respectively. Badeau [44], [72] introduced a unified mathematical framework to stochastically model the RIR, according to the source image principle [27]. This work reported that the image sources (i.e., reflections) are distributed according to a uniform Poisson distribution. The author further demonstrated that this stochastic distribution of image sources remains invariant regardless of the sound source's and receiver's locations and holds for a diffuse acoustic field. Alternatively, based on billiard theory, Polack [73] showed that the Poisson distribution of image sources is also independent of the room geometry. Furthermore, Traer and McDermott [74] analyzed the RIR statistics. They found that the time series of late reverberation of RIR exhibits a Gaussian distribution; this was in stark contrast to the time series of early reflection of RIR, which exhibited a non-Gaussian distribution. They also showed that the energetic exponential decay of the realistic RIR in late reverberation time series plays an important role in human perception of reverberation, rather early reflection has few effects on this. Moreover, Wang and Duangpummet [28], [29] demonstrated the efficacy of stochastic RIR modeling in the time domain, inspired by Schroeder's stochastic RIR model [75]. However, Schroeder's RIR model lacks representation of the onset transition (early reflections) in realistic RIR, as noted in [28], [29]. The extended RIR model in [28], [29] represents this onset transition of the RIR as a Gaussian process, which contradicts the sparse statistical property of early reflection in realistic RIRs [49]. Also, it is difficult to directly apply the mathematical framework proposed by [72] since we lack the imperative a priori knowledge about possible source image positions and attenuation coefficients set.

Depending on the findings of Badeau [72], Polack [73], and Traer and McDermott [74], and inspired by the works of Schroeder [55], Duangpummet et al. [29], and Wang et al. [28], we present a novel stochastic RIR model in the time domain, namely, the *sparse stochastic impulse response (SSIR)* model. This model combines the different statistical properties of the early-reflection and late-reverberation time series of the RIR. We model the time series of early reflection of RIR as a uniform Poisson distribution with their sparsity proportional to the room volume as $h_i(t) \sim P(\lambda|V|)$, according to [44], [72]. Conversely, the time series of late reverberation presents a Gaussian distribution as $h_d(t) \sim N(0, 1)$, inspired by [28], [29], [55], [74]. Here, $h_i(t)$ and $h_d(t)$ represent the early

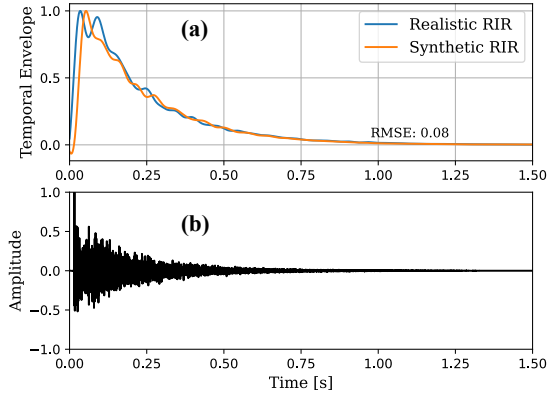


Fig. 3: Fitting of the SSIR model to the realistic RIR. (a) The temporal envelope of the realistic and synthetic RIRs. (b) The corresponding realistic RIR.

reflection and late reverberation of the RIR, respectively. V denotes the room volume. Fig. 3 shows the fitting of the proposed SSIR model to the realistic RIR.

The SSIR model can be defined as:

$$h_{\text{ssir}}(t) = \begin{cases} h_i(t) = be^{\alpha t/T_i} c_i(t), & t \in [0, T_i] \\ h_d(t) = be^{-\alpha t/T_d} c_d(t), & t \in [T_i, T_d] \end{cases} \quad (11)$$

$$c_i(t) \sim P(\lambda|V|) = \frac{\lambda^{|V|} \cdot e^{-\lambda}}{|V|!}, \quad (12)$$

$$c_d(t) \sim N(0, 1) = \frac{e^{-t^2/2}}{\sqrt{2\pi}}, \quad (13)$$

where T_i and T_d are two parameters that control the exponentially ascending and descending temporal envelopes of the RIR, respectively. $c_i(t)$ represents the carrier signal in the early reflection as the uniform Poisson-distributed noise, and $c_d(t)$ represents the carrier signal in the late reverberation as the standard Gaussian-distributed noise. The constant $\alpha = 6.9$ is known as Schroeder's coefficient, introduced in Schroeder's stochastic RIR model [75], [27, Ch.7], which determines the exponential decay and rising rate. λ is the parameter of the Poisson distribution, which is equal to μ that signifies the average value of T_i across the sample set. Here, μ is determined to be 0.0399 by averaging all T_i in the compiled RIR dataset mentioned in Sec. III-C1.

B. Datasets

A significant challenge encountered when using a data-driven method for the blind room acoustical estimation task lies in the quality and coverage of the collected data, which are crucial to ensure the ability of satisfactory generalization. Therefore, it is essential to construct a dataset characterized by large-scale quantity, substantial diversity, and detailed annotations of RAPs and RPPs. We employ a comprehensive collection of realistic RIRs from existing realistic RIR datasets. These RIRs cover a wide range of acoustic environments, featuring various volumes and geometries of the room, varied locations of the sound source and receiver, and different sound absorption coefficients of room surfaces. Hence, it can contain a wide spectrum of broadband RAPs and RPPs. Furthermore, the dataset is augmented to refine the distribution of the annotations, thus maximizing the diversity and representativeness of the dataset.

1) *RIR Data Collection*: We aggregated five extensive realistic RIR datasets to construct a composite RIR dataset to represent a wide range of room geometries and RACs. These datasets are the **Arni RIR dataset** [46], the **Motus dataset** [47], the **BUT ReverbDB** [76], the **ACE corpus of RIRs** [38], and the **OpenAIR dataset** [77]. Each dataset comprises monochanneled and omnidirectionally recorded RIRs. All the selected datasets contain the detailed attributes in terms of room volumes, including 39 different rooms with volumes from 30 m^3 to $47,000 \text{ m}^3$, locations of sound sources and receivers or equivalent information such as distances and DOAs of sound sources. We resampled all RIRs to 16 kHz.

2) *Speech and Noise Data Collection*: To replicate the environmental background noise encountered in real-world scenarios, instead of using synthetic white Gaussian noise, we use actual noise samples from real-world daily life circumstances. We integrate noise signals from the **DEMAND** [78] and **BUT** [76] noise datasets, both of which are collected in real-world environments of daily life and resampled at 16 kHz.

We use the LibriSpeech corpus [79] for sampling the sound source speech signals when synthesizing the observed reverberant signals. Specifically, we select a 360-hour clean subset. This subset is composed of more than 100,000 unique clips articulated by 921 speakers with completely distinct linguistic contents. The deployment of this dataset ensures a broad spectrum of diverse speech signals, enhancing the robustness and generalizability of our synthesized signals.

C. Data Preparation

1) *Synthesis of Noisy Reverberant Speech Signals*: In the composited RIR dataset with detailed annotations of T_i , T_d ; the parameters of the SSIR RIR model; and metrics related to room volume V , sound source distance D and DOA $\{\theta, \psi\}$ of the sound source, we further employ data augmentation strategy. The strategy involves *data upsampling* and *downsampling* techniques to modulate the distribution of the labels, which mitigates potential biases in the data distributions to obtain more natural distributions. For instance, RIRs measured in rooms with less frequently available volumes are disproportionately scarce. To address this imbalance, we downsampled RIRs associated with more prevalent room volume values while concurrently upsampling RIRs corresponding to the rarer volume values. The degrees of upsampling and downsampling are calibrated based on the relative rarity of the values of each label. This data augmentation strategy is open-sourced in the GitHub repository's data preprocessing procedure.⁴ After applying the data augmentation process to the RIR dataset, a comprehensive collection of 47,430 realistic RIRs is successfully compiled. This RIR dataset contains a wide range of RIRs, for which the corresponding T_{60} spans from 0.18 to 8.00 s (specifically, the lower and upper bounds are 0.188 and 7.958 s, respectively). The mean reverberation time (T_{60}) across this dataset is about 1.731 s.

Then, we randomly sampled 47,430 clips from the LibriSpeech corpus, choosing clips with the most common length (from 12 to 17 sec.) to be the sound source speech signals,

⁴https://github.com/Alized/BERP/blob/main/notebooks/dataset_preprocess.ipynb

regardless of the speaker information and linguistic content they contain. In parallel, noise signals are randomly sampled, following an independent and identically distributed (I.I.D.) pattern, from the DEMAND and BUT datasets. Then, in accordance with Eq. (8), we synthesize the noisy reverberant speech signals, in total 261 hours. To enhance the robustness and efficacy of the model across diverse noisiness environments, the signal-to-noise ratio (SNR) between the reverberant and noise signals is uniformly varied by adjusting the SNR at five different levels, ranging from 0 to 20 dB in 5 dB increments, including a scenario with no noise (Inf). Given the uniqueness of each clip, we guarantee that every synthesized speech signal maintains its individuality in terms of both its waveform and linguistic content, further augmenting the diversity and richness of the synthesized dataset.

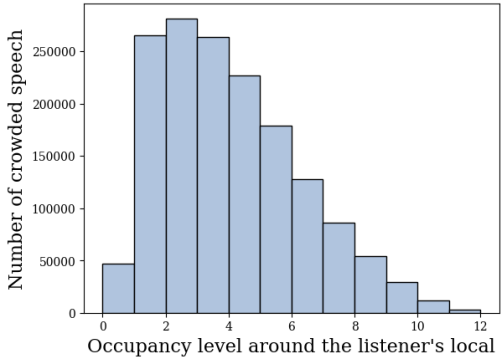


Fig. 4: Histogram of occupancy levels across crowded reverberant speech signals, adhering to a gamma distribution.

2) *Synthesis of Sparse Crowded Reverberant Speech Signals*: Initially, we apply voice activity detection to the LibriSpeech corpus to segment and annotate the timestamps corresponding to speech and silence segments. This process underlies the annotations of the synthesized crowded reverberant signals. Then, the discretized Gamma distribution of the occupancy levels is modeled using the mixtures of truncated Gaussian distributions, as detailed in Assumption 3 in Sec. III-A2. Explicitly, the different occupancy levels N in rooms of different volumes follow the different Gaussian distributions $N \sim N(N, 1)$. The choice of values of N of different volumes accompanies the real-world principle that larger spaces typically accommodate more occupants, while smaller spaces accommodate fewer occupants. These Gaussian distributions are mixed to approximate the discretized Gamma distribution of the occupancy levels across all room volumes.

Furthermore, the distribution of the distance d_i from the i -th occupant speaker to the listener is governed by a truncated Gaussian distribution (the Gaussian distribution that truncates its negative parts) $d_i \sim N(\mu_d, 1)$, where μ_d represents the median of the maximum (i.e., 6.0 m from Assumption 1 in Sec. III-A2) and minimum distances (i.e., d_0 , 1.0 m), which is decided as 2.5 m. The noise signals in this model are randomly sampled from the collected noise dataset mentioned in Sec. III-B2. Then, based on Eq. (10), we synthesize the sparse crowded reverberant signals. The SNR of the background noise is uniformly adjusted in five levels from 30 dB to 50 dB in the 5 dB step, to align with Assumption 1 that the background noise originates away from the 6 meter circular area.

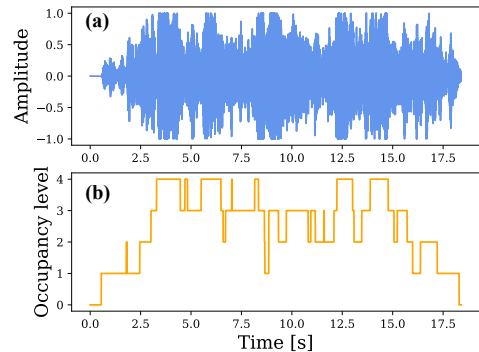


Fig. 5: An example of a crowded reverberant speech signal. (a) The crowded reverberant signal. (b) The corresponding instantaneous occupancy level (smoothed in frame 500 ms)

Using Eq.(10), we synthesize the sparse crowded reverberant speech signals by superimposing the speech signals uniformly sampled from the LibriSpeech corpus, aligning with the annotated speech and silence segmentation. The initiation index for each overlapping speech signal is determined based on an I.I.D. pattern. Additionally, to authentically replicate the local room acoustics, the room volumes in the RIRs are precisely matched with their corresponding RIRs, thereby ensuring a realistic acoustic environment. Finally, we obtain a dataset comprising 47,430 samples of crowded reverberant speech signals, ranging from 10 to 25 sec, in total 222 hours of audio. Fig. 5 shows an example of a sparse crowded reverberant speech signal and its corresponding occupancy level according to Eq. (10) and the aforementioned synthesis strategy.

D. Estimation Framework Architecture

1) *Featurization*: We use the four types of featurization methods to represent the observed input signals, including *spectrogram*, *Gammatonegram*, *MFCC*, and *mel spectrogram*. A Gammatonegram emphasizes the importance of low-frequency sections while a signal propagates within a room [35], [80]. While the MFCC characterizes the shape of the spectral envelope of a reverberant signal, closely related to the MTF of room acoustics [81]. The mel spectrogram rather mimics human subjective perceptions to the RACs. To clarify the potential benefits of auditory-perceptually-based time-frequency representation features for the blind estimation task of room parameters, we implement the spectrogram. Before passing through featurizer, the amplitudes of the input signals are normalized using peak normalization.

2) *Room Feature Representation Learning*: We use a room feature encoder (RFE) to learn room feature representations.

Room Feature Encoder. The RFE is structured into eight blocks, each block comprising four components. It incorporates a half-residual feedforward network, a multiheaded self attention, a convolutional network, and another half-residual feedforward network [82].

This encoder integrates CNNs and transformer models, both of which account for grasping local and global acoustic features, respectively, since Wang et al. [28] showed that the acoustical information spreads the overall tempo-spectro components of the reverberant signal. Such an integration makes it particularly well suited for learning the sophisticated mappings

between the noisy and crowded reverberant speech signals with complex waveforms and the desired room parameters.

The signal flow from the input feature representation x_i to the latent variable output y_i across each block is mathematically expressed as:

$$x_i^{\ddagger} = x_i + \frac{1}{2} \cdot \text{FFN}(x_i), \quad (14)$$

$$x_i^{\ddagger\ddagger} = x_i^{\ddagger} + \text{LayerNorm}[\text{MHSA}(x_i^{\ddagger})], \quad (15)$$

$$x_i^{\ddagger\ddagger\ddagger} = x_i^{\ddagger\ddagger} + \text{Conv}(x_i^{\ddagger\ddagger}), \quad (16)$$

$$y_i = \text{LayerNorm}[x_i^{\ddagger\ddagger\ddagger} + \frac{1}{2} \cdot \text{FFN}(x_i^{\ddagger\ddagger\ddagger})], \quad (17)$$

where **FFN** denotes the feedforward network, **MHSA** denotes the multiheaded self attention, **Conv** denotes the convolutional network, and **LayerNorm** represents the layer normalization operation, respectively.

Feedforward network. The feedforward network is composed of a layernorm layer, linear layers with 2048 hidden and 512 embedding dimensions with the swish activation function [83], and a dropout layer of 0.1 dropout rate. Fig. 6 visualizes the architecture of this module.

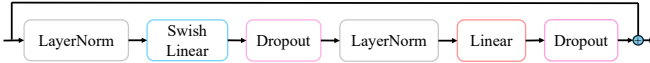


Fig. 6: Architecture of the feedforward network.

Multiheaded self attention. The multiheaded self attention with extrapolatable relative positional encoding (xPos) enhances the ability of the model to grasp the comprehensive global acoustical information encapsulated in feature representations [84]. Fig. 7 shows the corresponding architecture. The xPos encoding strategy has been empirically validated to augment the stabilization and robustness of the self attention mechanism, particularly for sequences with various lengths.

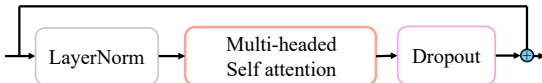


Fig. 7: Architecture of the multiheaded self attention.

The xPos-based relative self attention can be formulated as follows:

$$\text{RelAttn}(x) = \text{softmax} \left(\frac{\mathbf{Q}_{x,\text{xPos}} \mathbf{K}_{x,\text{xPos}}^T}{\sqrt{\mathcal{D}_h}} \mathbf{M} \right) \mathbf{V}_x \quad (18)$$

where $\mathbf{Q}_{x,\text{xPos}} = (\mathbf{W}_q \mathcal{C} + \mathfrak{R}_Q \mathcal{S}) \mathcal{T}$, $\mathbf{K}_{x,\text{xPos}} = (\mathbf{W}_k \mathcal{C} + \mathfrak{R}_K \mathcal{S}) \mathcal{T}^{-1}$, and $\mathbf{V}_x = \mathbf{W}_v x$. \mathcal{C} is equal to $\cos(m\vartheta_i)$ and \mathcal{S} is equal to $\sin(m\vartheta_i)$, which are the cosine and sine positions at the embedding dimension i and the time slice m , respectively. \mathfrak{R} corresponds to the rotary matrix of \mathbf{Q} and \mathbf{K} . \mathcal{D}_h is the head dimension of the attention mechanism. “ T ” denotes transposition. $\mathcal{T} = \varsigma_{m,i}$. The ς_i is given by:

$$\varsigma_i = \frac{i/\mathcal{D}_h + \beta}{1 + \beta}. \quad (19)$$

where β is the optimal setting and $\vartheta_i = 10000^{-2i/\mathcal{D}_h}$. \mathbf{W}_q , \mathbf{W}_k , \mathbf{W}_v and \mathbf{M} are trainable weighting matrices of query, key, and value of the attention mechanism, respectively.

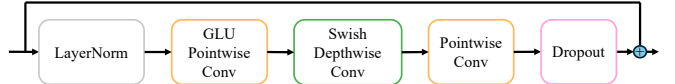


Fig. 8: Architecture of the convolutional network.

Convolutional network. The convolutional network functions in capturing the local acoustic features and reinforcing the temporal causality of the feature representation. This module leverages prenorm residual connection with gating mechanisms to distill the important acoustical characteristics via pointwise and depthwise convolutional and a gated linear unit (GLU) layers [85], as illustrated in Fig. 8.

3) Regression Estimation of the Room Parameters: For the regression task of room parameter estimation, we employ a parametric predictor (PP) solely for T_i , T_d , V , D , and use both PP and an acoustical bias corrector (ABC) for θ and ψ .

Parametric Predictor. The PP employs several convolutional layers with ReLU activation functions to compose a nonlinear regression function, allowing us to utilize the encoded representations within the latent space to predict the physically-meaningful room parameters. These parameters include the two parameters of the SSIR model \hat{T}_i and \hat{T}_d , the room volume \hat{V} , the sound source distance \hat{D} , and the DOA of the sound source $\hat{\theta}$ and $\hat{\psi}$. The behavior of the predictor can be mathematically determined as follows:

$$\gamma = f_{\text{pred}}(\mathbf{y}_{\text{enc}}) \quad (20)$$

where γ denotes the room parameters output from the PP, which is a constant function alongside the time axis, including T_i , T_d , V , D , θ , and ψ . \mathbf{y}_{enc} denote the hidden states output from the RFE. Specifically, the regressive function f_{pred} can be expressed as in a stepwise manner:

$$\mathbf{y} = \text{LayerNorm}[\max(0, \text{conv}(\mathbf{y}_{\text{enc}}))], \quad (21a)$$

$$\mathbf{y}' = \text{LayerNorm}[\max(0, \text{conv}(\mathbf{y}))], \quad (21b)$$

$$\tilde{\mathbf{y}} = \text{LayerNorm}[\max(0, \text{conv}(\mathbf{y}'))], \quad (21c)$$

$$\mathbf{y}'' = \text{LayerNorm}[\max(0, \text{conv}(\tilde{\mathbf{y}}))], \quad (21d)$$

$$\gamma = \mathbf{W}_l \mathbf{y}'' + \mathbf{b}_l, \quad (21e)$$

where **conv** denotes the convolutional layer designed to extract and process latent feature representations. The output linear layer, characterized by the trainable weight \mathbf{W}_l and bias \mathbf{b}_l , produces γ in Eq. (20). During inference, we sum up and average the values over the time axis to obtain a single predicted room parameter. The overall architecture of the PP is presented in Fig. 9. The estimated T_i , T_d , and V obtained from the dedicated PPs are utilized to synthesize the estimated RIRs, by using the SSIR model in Eq. (11), (12), and (13). The estimated RAPs are thus derived from the estimated RIRs by using the corresponding calculation methods detailed in Sec. II-A.

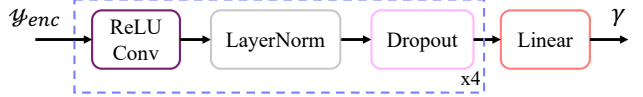


Fig. 9: Architecture of the PP.

Acoustical Bias Corrector. The ABC acts as a gating mechanism to differentiate between biased and unbiased data

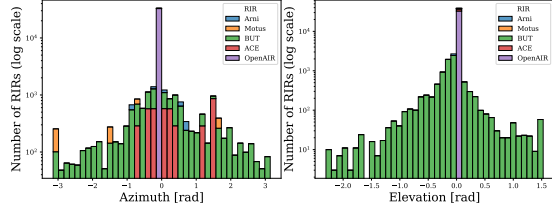


Fig. 10: Histogram of DOAs of the sound source.

encoded within the latent space, thereby directing the optimal signal flow into the PP and ensuring that the PP can learn from the unbiased data distribution. Additionally, we leak some biased data into the PP to make it robust to biases. The necessity of such a mechanism arises in the context of room parameters such as the sound source azimuth θ and elevation ψ , whose distributions exhibit the substantial inherent biases that are difficult to mitigate through conventional data augmentation techniques, as shown in Fig. 10. Biases often lead to the regression of trivial results, i.e., the mean of the whole distribution.

The ABC comprises a sandwich structure, characterizing the rotary-positional self attention [86] as a feature enhancer to assign the different attention weights to all latent spectro-temporal feature representation in a frame-by-frame manner. The rotary position encoding approach also contributes to stabilizing the training process. It is also adaptable to variable latent input lengths without the need for alignment. The output bias probability $p_{abc}(\hat{y})$ of the ABC from the output latent space of the RFE y_{enc} can be mathematically expressed as follows:

$$p_{abc}(\hat{y}) = f_{corr}(y_{enc}). \quad (22)$$

Fig. 11 depicts the entire architecture of the ABC. “GELU”



Fig. 11: Architecture of the ABC.

and “Sigmoid” denote the GELU [87] and sigmoid activation functions, respectively.

4) *Classification Estimation of the Room Parameters*: A FC layer is engineered to regress encoded feature representations to physics-informed instantaneous occupancy levels as a time sequence derived from the observed crowded signals. The pivot of this architecture is substantiated by **Assumption 2** (Section III-A2), which facilitates the prediction of a time series from a regression task to a classification task, thus simplifying the complexity of the task while improving the robustness of the prediction. Considering that the occupancy level exhibits no significant temporal dependence, we instead simply adopt a linear layer with log-softmax activation function to predict the occupancy level rather than recurrent or autoregressive structures. The resolution of the estimation process is about 62.5 Hz, i.e., 16 ms per frame, to predict the occupancy level around the listener’s location.

E. Joint Estimation Framework

We explore a joint estimation framework to estimate multiple RAPs and RPPs simultaneously. The underlying hypothesis

posits that the RAPs, which are directly derived from the RIR, share the same reverberation information encapsulated in the RIR. Additionally, the observed reverberant signal embodies crucial physical information related to volume and sound source characteristics. Furthermore, the interdependency between the RAPs and RPPs plays a pivotal role in improving the robustness and efficacy of the estimation, which is anticipated to improve the accuracy of the joint estimation strategy to be at least similar to that of the separate strategy. These hypotheses support the feasibility of developing a universal model, which is a promising approach to efficiently analyze room acoustics within a unified estimation framework rather than training multiple separate models.

The architecture of the joint estimation method is illustrated in Fig. 1. The *unified* and *occupancy modules* originate from the noisy reverberant signal y_{nr} and the crowded reverberant signal y_{cr} , respectively. Within the joint framework, the unified RFE serves as the foundational component across all PPs, facilitating the mutual exchange of interdependent information among the RAPs and RPPs in the latent space. Subsequently, each targeted room parameter is tasked with regressing a distinct function by using a dedicated predictor for desired room parameters. The configuration of each PP, as well as that of the ABC, is described in Section III-D3.

F. Loss Function

1) *Loss for the Parametric Predictor*: We employ Huber loss [88] to optimize PPs in each target room parameter. The Huber loss of the PPs is defined as:

$$\mathcal{L}_{\text{pred}}(\gamma, \hat{\gamma}) = \begin{cases} \frac{1}{2N} \sum_{n=1}^N \sum_{k=1}^K (\gamma_n - \hat{\gamma}_{n,k})^2, & |\gamma_n - \hat{\gamma}_{n,k}| \leq \delta \\ \delta \frac{1}{N} \sum_{n=1}^N \sum_{k=1}^K |\gamma_n - \hat{\gamma}_{n,k}| - \frac{1}{2} \delta^2, & |\gamma_n - \hat{\gamma}_{n,k}| > \delta \end{cases} \quad (23)$$

where γ is the targeted room parameter and δ is set to 1. The symbol N denotes the batch size and K represents the time frame length. The Huber loss possesses the dual sensitivity of the minimum-variance estimation by the $L2$ loss and the robustness of the median-aware estimation against outliers by the $L1$ loss. It also circumvents the convergence problem of the $L1$ loss on a small scale [89] and contributes to preventing exploding gradients by clipping gradients exceeding δ .

2) *Loss for the Acoustical Bias Corrector*: Considering the prediction task of the ABC is binary, i.e., distinguishing between unbiased and biased data, we adopt the binary cross-entropy (BCE) for optimization, which is defined as follows:

$$\mathcal{L}_{\text{corr}} = -\frac{1}{N} \sum_{n=1}^N y_n^{abc} \cdot \log(p_{abc}(\hat{y}_n)) + (1 - y_n^{abc}) \cdot \log(1 - p_{abc}(\hat{y}_n)), \quad (24)$$

where y_n^{abc} denotes the ground-truth label presenting acoustical bias, and $p_{abc}(\hat{y}_n)$ denotes the predicted bias probability output from the ABC.

3) *Loss for the Occupancy Module*: The occupancy module utilizes the cross-entropy (CE), reflecting the multiclass nature of the occupancy level estimation task. This loss function is determined as follows:

$$\mathcal{L}_{\text{occu}} = -\frac{1}{N} \sum_{n=1}^N \sum_{c=0}^C N_{n,c} \log(p_{\text{crowd}}(\hat{y}_{n,c}^{\text{crowd}})), \quad (25)$$

and \mathcal{C} , the upper bound of the occupancy level, is set to 12 according to Assumption 2 (detailed in Section III-A2). Here, $\hat{y}_{n,c}^{crowd}$ represents the logits output from the FC, p_{crowd} denotes the output probability after the softmax function, and $N_{n,c}$ denotes the instantaneous occupancy level of ground truth.

4) *See-Saw Loss*: When estimating the azimuth and elevation of the sound source, the ABC is deployed to counteract the significant bias inherent within the data distribution. Nevertheless, a critical issue arises from the disparate gradient descent rates of the two loss functions employed (the Huber and BCE losses). The gradient descent rate for the BCE loss is significantly faster than that for the Huber loss, causing the training instability, specifically when the BCE loss approaches overfitting, whereas the Huber loss still remains underfitting.

Therefore, we introduce a new loss function, namely, the see-saw loss, to solve this disparity. This loss function can adaptively balance the gradient descent rates of BCE and Huber losses, thus stabilizing the training process. The see-saw loss function devised for DOA estimation is formulated as follows:

$$\mathcal{L}_{\text{see-saw}}(\theta; \psi, \hat{\theta}; \hat{\psi}) = \mathfrak{w}'_{\text{corr}} (\mathcal{L}_{\text{corr}}^{\text{az}} + \mathcal{L}_{\text{corr}}^{\text{elev}}) + \frac{\mathfrak{w}'_{\text{pred}} [\mathfrak{w}'_{\text{pred}} \mathcal{L}_{\text{pred}}(\theta, \hat{\theta}) + \mathfrak{w}''_{\text{pred}} \mathcal{L}_{\text{pred}}(\psi, \hat{\psi})]}{1 + \mathfrak{w}''_{\text{corr}} (\mathcal{L}_{\text{corr}}^{\text{az}} + \mathcal{L}_{\text{corr}}^{\text{elev}})}, \quad (26)$$

where $\mathcal{L}_{\text{see-saw}}(\theta; \psi, \hat{\theta}; \hat{\psi})$ denotes the total loss. The components $\mathcal{L}_{\text{corr}}^{\text{az}}$ and $\mathcal{L}_{\text{corr}}^{\text{elev}}$ represent the BCE losses of azimuth and elevation through the ABC, respectively. $\mathcal{L}_{\text{pred}}(\theta, \hat{\theta})$ and $\mathcal{L}_{\text{pred}}(\psi, \hat{\psi})$ correspond to Huber losses for the azimuth and elevation using PPs. $\mathfrak{w}'_{\text{corr}}$ and $\mathfrak{w}''_{\text{corr}}$ are the weight coefficients of the bias correctors. $\mathfrak{w}_{\text{pred}}$, $\mathfrak{w}'_{\text{pred}}$, and $\mathfrak{w}''_{\text{pred}}$ are the corresponding weight coefficients of the predictors.

5) *Polynomial See-Saw Loss for Joint Estimation*: We introduce a loss function that combines polynomial losses with see-saw loss for the joint estimation framework.

The polynomial see-saw loss $\mathcal{L}_{\text{unified}}$ is formulated as follows:

$$\mathcal{L}_{\text{unified}}(T_i; T_d; V; D; \theta; \psi, \hat{T}_i; \hat{T}_d; \hat{V}; \hat{D}; \hat{\theta}; \hat{\psi}) = \mathfrak{w}_{T_i} \mathcal{L}_{\text{pred}}(T_i, \hat{T}_i) + \mathfrak{w}_{T_d} \mathcal{L}_{\text{pred}}(T_d, \hat{T}_d) + \mathfrak{w}_V \mathcal{L}_{\text{pred}}(V, \hat{V}) + \mathfrak{w}_D \mathcal{L}_{\text{pred}}(D, \hat{D}) + \mathcal{L}_{\text{see-saw}}(\theta; \psi, \hat{\theta}; \hat{\psi}), \quad (27)$$

where \mathfrak{w}_{T_i} , \mathfrak{w}_{T_d} , \mathfrak{w}_V , and \mathfrak{w}_D are weighting coefficients for losses $\mathcal{L}_{\text{pred}}(T_i, \hat{T}_i)$, $\mathcal{L}_{\text{pred}}(T_d, \hat{T}_d)$, $\mathcal{L}_{\text{pred}}(V, \hat{V})$, and $\mathcal{L}_{\text{pred}}(D, \hat{D})$, respectively. Through multiple experimental testing, the weighting ratio is optimally arranged as: $\mathfrak{w}_{T_i} : \mathfrak{w}_{T_d} : \mathfrak{w}_V : \mathfrak{w}_D : \mathfrak{w}'_{\text{corr}} : \mathfrak{w}''_{\text{corr}} : \mathfrak{w}'_{\text{pred}} : \mathfrak{w}''_{\text{pred}} = 5.0 : 5.0 : 5.0 : 5.0 : 0.1 : 0.1 : 0.5 : 10.0 : 1.0$.

G. Evaluation Metrics

We employ the mean absolute error (MAE) and the Pearson correlation coefficient (PCC) as the evaluation metrics. The MAE provides a direct measure of the scale of the average estimation error and the PCC is introduced to quantify the invariant similarity of the estimated and ground-truth values.

When estimating the occupancy levels as a time sequence, we choose only the MAE to quantify the Euclidean distance between the estimated and ground-truth occupancy sequences.

IV. EXPERIMENTS

A. Experimental Setup

Training strategy. We randomly split the 47,430 total distinct clips of noisy and crowded reverberant speech signals into three segments, training, validation, and test datasets, following the I.I.D. paradigm. We allocate 2000 clips each to the validation and test datasets and the remaining 43,430 clips are for the training dataset. The padding mask is deployed to ensure that the framework learns only the valid information across each minibatch. The RAdam optimizer with \mathcal{L}_2 regularization is used [90], which possesses a functionality of learning rate warmup without the risk of underfitting the regression tasks. We utilize cosine-annealing and tri-stage learning rate scheduler for unified and occupancy modules, respectively, to facilitate the convergence of the models toward the global optimums. We set a batch size of 12. Given the wide range of room volumes spanning from 40 to 9000 m^3 , we apply logarithmic scaling to compress them, stabilizing the training process and improving model robustness. Unitary linear normalization is applied to standardize the gradient update rate to ensure a uniform descent across labels.

Featurizer configuration. We set a uniform configuration for all spectrogram-variant featurizers. They each contain the same 128 frequency bins, Gammatone, mel filterbank, and DCT bins channels; Hanning windowing with a size of 1024; and a 75% overlapping rate.

Baselines. In our comparative experiments, we evaluated the performance of our proposed method compared to four baseline architectures that are renowned in the domain of room parameter estimation amidst background noise: the Full-CNN [33]–[35], the CRNN [36], [37], the TAE-CNN [29], and RE-NET [39]. We adopt the configurations of Full-CNN and CRNN architectures based on their latest variants as described in [33] and [36], respectively. To ensure fair comparisons, we retrained all baselines using the same compiled noisy reverberant datasets mentioned in Sec. III-B for the room parameters T_i , T_d , V , D , θ , ψ that are output from trained models. All baselines were sufficiently trained for convergence. These SOTA frameworks were deployed in joint and separate estimation tasks.

B. Results

1) *Evaluation of the Room Parameters Derived from Frameworks*: We evaluated the proposed BERP and the baseline frameworks using the same dataset as detailed in Sec. III-C1 and the same data segmentation setting for the joint estimation of the room parameters T_i , T_d , V , D , θ , ψ and N output from trained models.

Table I shows the estimation accuracies achieved by the BERP across three featurizations, alongside a comparison with the baselines. BERP significantly outperforms SOTA architectures in terms of MAE and PCC evaluation metrics. Even for parameters such as azimuth θ and elevation ψ , which are subject to significant data distribution biases, the BERP maintains its effectiveness. Moreover, the performance comparison among the three featurizers indicates that the MFCC featurizer yields the most favorable outcomes, which

TABLE I: MAE and PCC comparisons among variants of the proposed BERPs with different featurizations and baselines for the room parameters derived from the estimation frameworks, i.e., the neural network models. All models, including BERPs and baselines, were sufficiently trained until convergence. Gammatone, Mel, and MFCC denote the featurization methods.

		T_i (joint) [s]	T_d [s]	V [$\log_{10}(m^3)$]	D [m]	θ [rad]	ψ [rad]	N
MAE ↓	Full-CNN [33]–[35]	1.7720	1.0050	1.3210	3.8260	3.2610	0.5966	-
	CRNN [36], [37]	0.0238	0.2968	0.3189	1.8730	0.3685	0.1002	-
	TAE-CNN [29]	0.0404	0.4608	0.4328	3.8700	0.3157	0.0684	-
	RE-NET [39]	0.1844	1.1460	0.5102	4.6180	0.8614	0.8183	-
	BERP-Spectrogram	0.0025	0.0325	0.0419	0.7089	0.0628	0.0242	0.5952
	BERP-Gammatone	0.0030	0.0341	0.0373	0.6918	0.0780	0.0218	0.5582
	BERP-Mel	0.0018	0.0221	0.0272	0.5070	0.0626	0.0221	0.5534
PCC ↑	BERP-MFCC	0.0019	0.0264	0.0271	0.5375	0.6066	0.0236	0.5590
	Full-CNN [33]–[35]	0.1543	0.6431	0.3268	0.5731	0.0329	0.0116	-
	CRNN [36], [37]	0.6914	0.9356	0.7450	0.8512	0.1157	0.1756	-
	TAE-CNN [29]	-	-	0.5555	0.5194	-	-	-
	RE-NET [39]	0.2395	0.1579	0.3961	0.3285	0.0629	0.1579	-
	BERP-Spectrogram	0.9546	0.9942	0.9595	0.9310	0.7218	0.7225	-
	BERP-Gammatone	0.9437	0.9929	0.9731	0.9271	0.6311	0.6936	-
PCC ↑	BERP-Mel	0.9691	0.9971	0.9705	0.9503	0.7017	0.7342	-
	BERP-MFCC	0.9667	0.9951	0.9733	0.9520	0.7290	0.7380	-

TABLE II: Evaluation results obtained for the RAPs derived from the SSIR RIR model of the proposed BERP.

		STI	%AL _{cons}	T_{60} [s]	EDT	C_{80} [dB]	C_{50} [dB]	D_{50} [%]	T_s [s]
MAE ↓	BERP-Spectrogram	0.0537	4.0728	0.0326	0.3312	2.9374	3.3308	14.6316	0.0527
	BERP-Gammatone	0.0544	4.1388	0.0342	0.3378	2.966	3.3556	14.7659	0.0539
	BERP-Mel	0.0534	4.0794	0.0221	0.3282	2.9051	3.3135	14.5699	0.0528
	BERP-MFCC	0.0540	4.0877	0.0265	0.3325	2.9498	3.3418	14.6950	0.0532
PCC ↑	BERP-Spectrogram	0.9478	0.8649	0.9964	0.9859	0.9057	0.8385	0.8242	0.9762
	BERP-Gammatone	0.9477	0.8660	0.9976	0.9870	0.9047	0.8370	0.8221	0.9772
	BERP-Mel	0.9501	0.8682	0.9994	0.9892	0.9097	0.8412	0.8263	0.9802
	BERP-MFCC	0.9490	0.8671	0.9960	0.9864	0.9082	0.8397	0.8251	0.9777

TABLE III: Results of an ablation study concerning **separate estimation pipelines**. The MAE and PCC attained by the proposed BERP and the baselines in separate estimation pipelines are presented. All models, including baselines and BERP, were sufficiently trained until convergence. We used the MFCC featurization method for the BERP.

		T_i (separate) [s]	T_d [s]	V [$\log_{10}(m^3)$]	D [m]	θ [rad]	ψ [rad]
MAE ↓	Full-CNN [33]–[35]	0.0704	0.3085	0.5282	4.8520	0.3139	0.0702
	CRNN [36], [37]	0.0177	0.2927	0.1597	1.6540	0.2583	0.0701
	TAE-CNN [29]	0.0341	1.7320	3.1200	7.704	0.3157	0.0683
	RE-NET [39]	0.0341	0.6283	0.4963	5.2390	0.3140	0.0733
	BERP	0.0025	0.0322	0.0382	0.6413	0.0722	0.0183
PCC ↑	Full-CNN [33]–[35]	0.2660	0.9377	-	-	-	-
	CRNN [36], [37]	0.5202	0.9481	0.9221	0.8859	0.3397	0.2612
	TAE-CNN [29]	-	-	-	-	-	-
	RE-NET [39]	0.1159	0.6722	0.3293	0.1243	0.0341	0.0296
PCC ↑	BERP	0.9597	0.9976	0.9641	0.9336	0.6173	0.6595

TABLE IV: Results of an ablation study concerning **disentangling PP**. The PP is replaced with a simple linear layer to investigate the contribution of the PP. The MFCC featurization is employed across all evaluations.

	Architecture	T_i	T_d	V	D
(separate)					
MAE ↓	BERP w/o PP	0.1620	1.0023	0.0508	0.5960
	BERP	0.0025	0.0322	0.0382	0.6413
(joint)					
MAE ↓	BERP w/o PP	0.1174	1.1707	0.4173	8.4852
	BERP	0.0019	0.0264	0.0271	0.5375
PCC ↑	BERP w/o PP	0.6013	0.9211	0.9554	0.9343
	BERP	0.9579	0.9948	0.9641	0.9336

supports our assertion regarding the intrinsic relevance of MFCC to room acoustics, highlighting its fitness to blind estimation of room parameter.

2) *Evaluation of the Room Acoustic Parameters Using the SSIR Model:* Table II shows the estimation results obtained for the RAPs derived from the synthesized RIR using the SSIR RIR model. These results indicate the effectiveness of the SSIR for modeling realistic RIRs and subsequently deriving RAPs, highlighting the ability of the SSIR model to capture the essence of real-world RIRs for the precise estimation of RAPs. Specifically, when applied to the mel spectrogram featurizer, the BERP achieves better performance.

3) *Ablation Study: Separate estimation pipelines.* To further investigate the efficacy of our specifically designed *RFE*, *PP*, and *ABC* to estimate the RAPs and RPPs, we employed the separate estimation tasks. It is also conducted to verify our hypothesis asserted in Section III-E, in which the unified encoder promotes the effectiveness of the estimation. This ablation study comprises four separate pipelines, each of which

TABLE V: Results of an ablation study concerning **the efficacy of the ABC**. We utilize BERPs with and without the ABC to investigate the efficiency of the ABC used in the orientation module only. The featurization method is MFCC. The ABC significantly improves the task of regressing azimuth and elevation parameters with inherent distribution biases.

	Orientation Module	θ	ψ
PCC \uparrow	BERP w/o ABC	0.4863	0.4244
	BERP	0.6173	0.6595
MAE \downarrow	BERP w/o ABC	0.0704	0.0848
	BERP	0.0722	0.0183

is dedicated to mapping the observed speech signals to the corresponding target RAPs and RPPs, which include the *RIR*, *volume*, *distance*, and *orientation* modules. The RIR module concurrently estimates the two parameters T_i and T_d of the SSIR model. The volume and distance modules estimates the room volume V and the sound source distance D , respectively. Finally, the orientation module tests the task of simultaneously estimating the DOA of the sound source, i.e., θ and ψ . The results are shown in Table III, showing that the BERP also significantly outperforms the current methods. These results indicate that the proposed framework is effective even though in separate estimations. They also substantiate our hypothesis that joint estimation enhances the estimation accuracy via the mutual interdependence of room parameters and facilitates the sufficient and efficient learning for the neural networks.

Without the parametric predictor. To dissect the contribution of the PP to the overall performance of the BERP, we conducted the ablation study. We employed the separate pipelines for the three modules, *RIR*, *volume*, and *distance* modules. The joint framework is also tested by discarding the estimation of the DOA since the *orientation* module integrates the ABC. We consistently used the MFCC featurizer. Table IV compares the results obtained using solely the RFE with those achieved by using the full architecture equipped with the PP. The results show that the PP contributes significantly to the performance of the BERP, especially in the joint estimation.

Without the acoustical bias corrector. To understand the efficacy of the ABC, we conducted an ablation study with or without this bias corrector in terms of estimating the sound source azimuth θ and elevation ψ . Importantly, the PCC is much more representative than the MAE for evaluating the performance achieved on datasets with biased data distributions. Table V indicates that the ABC significantly mitigates the intrinsic bias within the dataset, proving the efficacy of the ABC for use with substantially biased data distributions.

4) *Evaluation on Recorded Reverberant Signals:* To further validate the cross-dataset generalization capability of the proposed framework, including the dataset augmentation pipeline and the neural network model, we evaluated the trained weights using reverberant speech signals recorded in realistic room acoustics. It is noteworthy that such evaluations using real recorded speech signals are seldom conducted in related works [29], [33]–[37] due to the scarcity of real recorded reverberant speech corpora and the significant expense associated with creating such datasets. For this purpose, we used the BUT retransmission speech corpus [76] that records the transmitted

speech signals through 267 RIR configurations. We compared our approach with baselines trained on the same compiled dataset, evaluating room parameters including T_i , T_d , V , D , θ , and ψ . Regarding the occupancy level N , to the best of our knowledge, no recorded speech dataset is available for blind estimation of occupancy levels. Creating such a dataset is further conducted in future work.

Table VI presents the evaluation results of all trained weights on the recorded reverberant speech signals. BERP significantly outperforms state-of-the-art baselines, demonstrating its generalizability to real recorded reverberant speech. However, we notice some deterioration in generalization performance compared to the evaluation on synthesized reverberant data. We conclude that while the synthesis of observed reverberant signals assumes a linear time-invariant (LTI) system, real-world acoustic environments do not strictly comply with this ideal LTI assumption. This deviation may contribute to the gap between the sim-to-real transfer of the trained models. This suggests that training or finetuning with real recorded reverberant signals might lead to better generalization performance, which we intend to explore in future work.

V. CONCLUSION

We propose the BERP, a universal blind estimation framework designed for simultaneously estimating several RAPs and RPPs, i.e., speech transmission index (STI), articulation loss of consonants (%AL_{cons}), reverberation time (T_{60}), early decay time (EDT), clarity (C_{80} and C_{50}), definition (D_{50}), center time (T_s), room volume (V), sound source distance D , DOA of the sound source (θ and ψ), and instantaneous occupancy level (N). The BERP provides a new paradigm for blind estimation in room acoustics. This framework can blindly evaluate RAPs and RPPs simultaneously within a wide range of realistic acoustical environments to parameterize the listener's local RACs, promising that it has a wide variety of applications in room acoustics, hearing aids, communications, and human-machine interactions [6], [13]–[17], [19], [21]–[26], [91]. We incorporate a new stochastic RIR model, namely the SSIR model, to realize the concurrent and efficient estimation of RAPs without increasing the computational complexity of the framework. This scheme avoids the use of complicated optimization processes across the significant disparity of the values of the different RAPs. Moreover, BERP fills the gap in the domain, i.e., the lack of a universal framework for blindly estimating these room parameters from single-channel noisy speech signals, especially for the sound source distance, DOA of the sound source, and instantaneous occupancy level. The evaluation results show that the proposed BERP framework outperforms the current methods greatly and achieves SOTA performance by simultaneously estimating thirteen room-acoustics-related parameters for the first time.

Differences between the proposed framework and the baselines. This subsection tries to answer two key questions: 1) what is the algorithmic difference from the baselines; 2) why the proposed framework outperforms. Functionally, a noticeable distinction is the framework's ability to predict instantaneous occupancy level N with high accuracy over

TABLE VI: Results of evaluation concerning the effectiveness and generalization of the trained weights in the real recorded reverberant speech signals. The MAE and PCC are reported for the proposed BERP with different featurization methods and the baselines. All the models were sufficiently trained to convergence.

		T_i [s]	T_d [s]	V [$\log_{10}(m^3)$]	D [m]	θ [rad]	ψ [rad]
MAE ↓	Full-CNN [33]–[35]	1.5792	0.7862	0.7759	2.8350	0.3133	0.1469
	CRNN [36], [37]	0.0204	0.3605	0.6949	4.5553	0.2983	0.1099
	TAE-CNN [29]	0.0267	0.8396	0.7375	2.1685	0.2941	0.1135
	RE-NET [39]	0.5742	1.6449	0.4131	5.4775	0.6130	0.6941
	BERP-Spectrogram	0.0120	0.1375	0.1959	1.7212	0.2956	0.1304
	BERP-Gammatone	0.0114	0.0989	0.1571	1.6736	0.4436	0.1245
	BERP-Mel	0.0077	0.1128	0.0511	1.7972	0.2931	0.1084
PCC ↑	BERP-MFCC	0.0094	0.1166	0.0821	1.9067	0.3126	0.1315
	Full-CNN [33]–[35]	0.6468	0.9091	0.1585	0.2661	-	-
	CRNN [36], [37]	0.4671	0.8386	0.0996	0.1926	0.1926	0.0116
	TAE-CNN [29]	-	0.8396	0.2282	0.4406	-	-
	RE-NET [39]	-	-	-	-	-	-
	BERP-Spectrogram	0.6034	0.9673	0.7444	0.5017	0.3332	0.2626
	BERP-Gammatone	0.7018	0.9570	0.6901	0.5074	0.3030	0.3841
	BERP-Mel	0.7562	0.9433	0.9052	0.5529	0.3995	0.4344
	BERP-MFCC	0.7562	0.9875	0.9007	0.4156	0.3359	0.3980

very short time windows (16 ms), a capability lacking in the baselines due to our modular design and the naturally a sequence-to-sequence model. Algorithmically, the proposed framework differs in architecture and internal mechanism. We adopt a modular design, separating the frontend (universal encoder) from the backend (parallel parametric predictors), unlike the integrated design of previous methods. This design enables efficient learning of room features through the universal encoder, particularly enhanced by multitask learning with multiple losses, as shown in Sec. IV-B3. Second, it enables a focused regression of each room parameter without mutual interference. Our framework can also handle arbitrary-length input signals without length alignment compared to all previous methods. On the other hand, our framework combines self attention with convolutions, which allows for grasping the global dependencies and local structure in the data, unlike previous methods' focus on the local patterns only by using convolutions solely [29], [33]–[35], [39] or fusion of convolution and unidirectional RNN [36], [37]. This combination also reduces the strong inductive bias brought about by the convolutions to better performance by introducing global views. Additionally, our framework allows for efficient capture of global and position-relative local interactions throughout the sequence, suitable for estimation of room acoustics that affects entire observed signals.

Limitations and Future work. Regarding the limitations of this study and future work, important, except for occupancy level estimation, the BERP assumes a dynamic-movement, single-source speech signal as the observed input. Future research will aim to address the blind estimation of RAPs and RPPs for multisource speech signals by developing a unified signal model that can accommodate both noisy and crowded reverberant signals in real-world environments. Additionally, we will explore to blend the real recorded speech signals to improve the generalization performance of the framework. These extensions will further expand the applicability of the proposed framework to more complex realistic scenarios.

VI. ACKNOWLEDGEMENTS

We appreciate the great help from Jinan Chen for this work.

REFERENCES

- [1] M. Barron, *Auditorium Acoustics and Architectural Design* (2nd ed.). London: Routledge, 2009.
- [2] ISO 3382:2009, *Acoustics - measurements of room acoustics parameters - Part 1: Performance spaces*. International Organization for Standardization, 2009.
- [3] A. Tsilfidis, I. Mporas, J. Mourjopoulos, and N. Fakotakis, "Automatic speech recognition performance in different room acoustic environments with and without dereverberation preprocessing," *Computer Speech & Language*, vol. 27, no. 1, pp. 380–395, 2013. Special issue on Paralinguistics in Naturalistic Speech and Language.
- [4] T. Jenrungrat, V. Jayaram, S. Seitz, and I. Kemelmacher-Shlizerman, "The cone of silence: Speech separation by localization," in *Advances in Neural Information Processing Systems*, 2020.
- [5] S. E. Chazan, H. Hammer, G. Hazan, J. Goldberger, and S. Gannot, "Multi-microphone speaker separation based on deep DOA estimation," 2019 27th European Signal Processing Conference (EUSIPCO), pp. 1–5, 2019.
- [6] J.-M. Jot and K. S. Lee, "Augmented reality headphone environment rendering," in *Audio Engineering Society Conference: 2016 AES International Conference on Audio for Virtual and Augmented Reality*, Sep 2016.
- [7] J. van der Werff and D. de Leeuw, "What you specify is what you get (part 1)," in *Audio Engineering Society Convention 114*, Mar 2003.
- [8] S. V. Amengual Garí, W. Lachenmayr, and E. Mommertz, "Spatial analysis and auralization of room acoustics using a tetrahedral microphone," *The Journal of the Acoustical Society of America*, vol. 141, pp. EL369–EL374, 04 2017.
- [9] C. Chen, U. Jain, C. Schissler, S. V. A. Gari, Z. Al-Halah, V. K. Ithapu, P. Robinson, and K. Grauman, "Soundspaces: Audio-visual navigation in 3D environments," in *Computer Vision – ECCV 2020: 16th European Conference, Glasgow, UK, August 23–28, 2020, Proceedings, Part VI*, (Berlin, Heidelberg), p. 17–36, Springer-Verlag, 2020.
- [10] A. Xenaki, J. Bünsow Boldt, and M. Græsbøll Christensen, "Sound source localization and speech enhancement with sparse Bayesian learning beamforming," *The Journal of the Acoustical Society of America*, vol. 143, pp. 3912–3921, 06 2018.
- [11] IEC 60268-16:2020, *Sound system equipment - part 16: Objective rating of speech intelligibility by speech transmission index*. International Electrotechnical Commission, 2020.
- [12] V. M. A. Peutz and W. Kelin, "Articulation loss of consonants influenced by noise," *Reverberation and Echo*, (in Dutch), vol. 28, pp. 11–18, 1974.
- [13] K. Kinoshita, M. Delcroix, T. Yoshioka, T. Nakatani, E. Habets, R. Haeb-Umbach, V. Leutnant, A. Sehr, W. Kellermann, R. Maas, S. Gannot, and B. Raj, "The reverb challenge: A common evaluation framework for dereverberation and recognition of reverberant speech," in *2013 IEEE Workshop on Applications of Signal Processing to Audio and Acoustics*, pp. 1–4, 2013.
- [14] L. Frenkel, S. E. Chazan, and J. Goldberger, "Domain adaptation using suitable pseudo labels for speech enhancement and dereverberation," *IEEE/ACM Transactions on Audio, Speech, and Language Processing*, vol. 32, pp. 1226–1236, 2024.

[15] H. Morgenstern and B. Rafaely, "Spatial reverberation and dereverberation using an acoustic multiple-input multiple-output system," *Journal of the Audio Engineering Society*, vol. 65, p. 42–55, Feb. 2017.

[16] T. Gajecki and W. Nogueira, "A fused deep denoising sound coding strategy for bilateral cochlear implants," *IEEE Transactions on Biomedical Engineering*, pp. 1–11, 2024.

[17] E. P. Reynders, J. Van den Wyngaert, M. Verlinden, and G. Vermeir, "Development and performance assessment of sound absorbing chandeliers for reverberation control and improved verbal communication in large rooms," *Applied Acoustics*, vol. 218, p. 109874, 2024.

[18] D. Fogerty, A. Alghamdi, and W.-Y. Chan, "The effect of simulated room acoustic parameters on the intelligibility and perceived reverberation of monosyllabic words and sentences," *The Journal of the Acoustical Society of America*, vol. 147, pp. EL396–EL402, 05 2020.

[19] B. Eurich, T. Klenzner, and M. Oehler, "Impact of room acoustic parameters on speech and music perception among participants with cochlear implants," *Hearing Research*, vol. 377, pp. 122–132, 2019.

[20] H.-Y. Lee, J.-W. Cho, M. Kim, and H.-M. Park, "Dnn-based feature enhancement using doa-constrained ica for robust speech recognition," *IEEE Signal Processing Letters*, vol. 23, no. 8, pp. 1091–1095, 2016.

[21] G. Yenduri, R. M. P. K. R. Maddikunta, T. R. Gadekallu, R. H. Jhaveri, A. Bandi, J. Chen, W. Wang, A. A. Shirawalmath, R. Ravishankar, and W. Wang, "Spatial computing: Concept, applications, challenges and future directions," 2024.

[22] H. M. Kamdjou, D. Baudry, V. Havard, and S. Ouchani, "Resource-constrained extended reality operated with digital twin in industrial internet of things," *IEEE Open Journal of the Communications Society*, vol. 5, pp. 928–950, 2024.

[23] J. Nikunen and T. Virtanen, "Direction of arrival based spatial covariance model for blind sound source separation," *IEEE/ACM Transactions on Audio, Speech, and Language Processing*, vol. 22, no. 3, pp. 727–739, 2014.

[24] A. Taghipour, S. Athari, A. Gisladottir, T. Sievers, and K. Eggenschwiler, "Room acoustical parameters as predictors of acoustic comfort in outdoor spaces of housing complexes," *Frontiers in Psychology*, vol. 11, p. 344, 03 2020.

[25] H. Dong and C. Lee, "Speech intelligibility improvement in noisy reverberant environments based on speech enhancement and inverse filtering," *J AUDIO SPEECH MUSIC PROC.*, vol. 3, 2018.

[26] X. Li, L. Girin, F. Badeig, and R. Horaud, "Reverberant sound localization with a robot head based on direct-path relative transfer function," in *2016 IEEE/RSJ International Conference on Intelligent Robots and Systems (IROS)*, p. 2819–2826, IEEE Press, 2016.

[27] H. Kuttruff, *Room Acoustics*. Taylor & Francis, 2016.

[28] L. Wang, S. Duangpummet, and M. Unoki, "Blind estimation of speech transmission index and room acoustic parameters by using extended model of room impulse response derived from speech signals," *IEEE Access*, vol. 11, pp. 49431–49444, 2023.

[29] S. Duangpummet, J. Karnjana, W. Kongprawechnon, and M. Unoki, "Blind estimation of speech transmission index and room acoustic parameters based on the extended model of room impulse response," *Applied Acoustics*, vol. 185, p. 108372, 2022.

[30] S. S. Kushwaha, I. R. Roman, M. Fuentes, and J. P. Bello, "Sound source distance estimation in diverse and dynamic acoustic conditions," in *2023 IEEE Workshop on Applications of Signal Processing to Audio and Acoustics (WASPAA)*, pp. 1–5, 2023.

[31] P.-A. Grumiaux, S. Kitić, L. Girin, and A. Guérin, "A survey of sound source localization with deep learning methods," *The Journal of the Acoustical Society of America*, vol. 152, pp. 107–151, 07 2022.

[32] C. Molnar and T. Freiesleben, *Supervised Machine Learning For Science*. 2024.

[33] C. Ick, A. Mehrabi, and W. Jin, "Blind acoustic room parameter estimation using phase features," in *ICASSP 2023 - 2023 IEEE International Conference on Acoustics, Speech and Signal Processing (ICASSP)*, pp. 1–5, 2023.

[34] A. F. Genovese, H. Gamper, V. Pulkki, N. Raghuvanshi, and I. J. Tashev, "Blind Room volume estimation from single-channel noisy speech," in *ICASSP 2019 - 2019 IEEE International Conference on Acoustics, Speech and Signal Processing (ICASSP)*, pp. 231–235, 2019.

[35] H. Gamper and I. J. Tashev, "Blind reverberation time estimation using a convolutional neural network," in *2018 16th International Workshop on Acoustic Signal Enhancement (IWAENC)*, pp. 136–140, 2018.

[36] P. S. López, P. Callens, and M. Cernak, "A universal deep room acoustics estimator," in *2021 IEEE Workshop on Applications of Signal Processing to Audio and Acoustics (WASPAA)*, pp. 356–360, 2021.

[37] P. Callens and M. Cernak, "Joint blind room acoustic characterization from speech and music signals using convolutional recurrent neural networks," ArXiv, vol. abs/2010.11167, 2020.

[38] J. Eaton, N. Gaubitch, A. Moore, and P. Naylor, "Estimation of room acoustic acparameters: The ACE challenge," *IEEE/ACM Transactions on Audio, Speech, and Language Processing*, vol. 24, pp. 1–1, 06 2016.

[39] K. Zheng, C. Zheng, J. Sang, Y. Zhang, and X. Li, "Noise-robust blind reverberation time estimation using noise-aware time-frequency masking," *Measurement*, vol. 192, p. 110901, 2022.

[40] M. Neri, A. Politis, D. A. Krause, M. Carli, and T. Virtanen, "Speaker Distance Estimation in Enclosures From Single-Channel Audio," *IEEE/ACM Transactions on Audio, Speech, and Language Processing*, vol. 32, pp. 2242–2254, 2024.

[41] N. Raghuvanshi, R. Narain, and M. C. Lin, "Efficient and accurate sound propagation using adaptive rectangular decomposition," *IEEE Transactions on Visualization and Computer Graphics*, vol. 15, no. 5, pp. 789–801, 2009.

[42] R. Scheibler, E. Bezzam, and I. Dokmanić, "Pyroomacoustics: A python package for audio room simulation and array processing algorithms," in *2018 IEEE International Conference on Acoustics, Speech and Signal Processing (ICASSP)*, pp. 351–355, 2018.

[43] E. Habets, "Room impulse response generator," 01 2006.

[44] R. Badeau, "Unified stochastic reverberation modeling," in *2018 26th European Signal Processing Conference (EUSIPCO)*, pp. 2175–2179, 2018.

[45] C. Christensen, G. Koutsouris, and J. Rindel, "The iso 3382 parameters: Can we simulate them? can we measure them?," vol. 20, 06 2013.

[46] K. Prawda, S. J. Schlecht, and V. Välimäki, "Calibrating the Sabine and Eyring formulas," *The Journal of the Acoustical Society of America*, vol. 152, pp. 1158–1169, 08 2022.

[47] G. Götz, S. J. Schlecht, and V. Pulkki, "A dataset of higher-order ambisonic room impulse responses and 3D models measured in a room with varying furniture," in *2021 Immersive and 3D Audio: from Architecture to Automotive (I3DA)*, pp. 1–8, 2021.

[48] A. Krizhevsky, I. Sutskever, and G. E. Hinton, "Imagenet classification with deep convolutional neural networks," *Commun. ACM*, vol. 60, p. 84–90, may 2017.

[49] J. Traer and J. H. McDermott, "Statistics of natural reverberation enable perceptual separation of sound and space," *Proceedings of the National Academy of Sciences*, vol. 113, no. 48, pp. E7856–E7865, 2016.

[50] R. Kliper, H. Kayser, D. Weinshall, I. Nelken, and J. Anemüller, "Monaural azimuth localization using spectral dynamics of speech," in *Proc. Interspeech 2011*, pp. 33–36, 2011.

[51] R. Takashima, T. Takiguchi, and Y. Ariki, "Single-channel multi-talker-localization based on maximum likelihood," in *2009 IEEE/SP 15th Workshop on Statistical Signal Processing*, pp. 461–464, 2009.

[52] F. Toole, *Sound Reproduction: The Acoustics and Psychoacoustics of Loudspeakers and Rooms*. Audio Engineering Society Presents, Taylor & Francis, 2017.

[53] S. Cerdá, A. Giménez, J. Romero, R. Cibrián, and J. Miralles, "Room acoustical parameters: A factor analysis approach," *Applied Acoustics*, vol. 70, no. 1, pp. 97–109, 2009.

[54] M. Queiroz, F. Iazzetta, F. Kon, M. H. A. Gomes, F. L. Figueiredo, B. Masiero, L. K. Ueda, L. Dias, M. H. C. Torres, and L. F. Thomaz, "Acmus: An open, integrated platform for room acoustics research - journal of the brazilian computer society," 2013.

[55] T. Houtgast and H. J. M. Steeneken, "The modulation transfer function in room acoustics as a predictor of speech intelligibility," *The Journal of the Acoustical Society of America*, vol. 54, no. 2, pp. 557–557, 1973.

[56] H. J. M. Steeneken and T. Houtgast, "A physical method for measuring speech-transmission quality," *The Journal of the Acoustical Society of America*, vol. 67, no. 1, pp. 318–326, 1980.

[57] T. Houtgast and H. J. M. Steeneken, "A review of the MTF concept in room acoustics and its use for estimating speech intelligibility in auditoria," *The Journal of the Acoustical Society of America*, vol. 77, pp. 1069–1077, 03 1985.

[58] M. R. Schroeder, "New method of measuring reverberation time," *The Journal of the Acoustical Society of America*, vol. 37, no. 3, pp. 409–412, 1965.

[59] J. S. Bradley, "Predictors of speech intelligibility in rooms," *The Journal of the Acoustical Society of America*, vol. 80, pp. 837–845, 09 1986.

[60] J. Bradley, R. Reich, and S. Norcross, "A just noticeable difference in C50 for speech," *Applied Acoustics*, vol. 58, no. 2, pp. 99–108, 1999.

[61] E. Meyer and R. Thiele, "Raumakustische untersuchungen in zahlreichen konzertsälen und rundfunkstudios unter anwendung neuerer Meßverfahren," *Acustica (In German)*, 1956.

[62] R. Kürer, "Einfaches messverfahren zur bestimmung der "schwerpunktseit" raumakustischer impulsantworten," *Proc Seventh Intern Congr on Acoustics (In German)*, 1971.

[63] O. Shih and A. Rowe, "Occupancy estimation using ultrasonic chirps," in Proceedings of the ACM/IEEE Sixth International Conference on Cyber-Physical Systems, ICCPS '15, (New York, NY, USA), p. 149–158, Association for Computing Machinery, 2015.

[64] H. Qian, G. Zhenhao, and L. Chao, "Occupancy estimation in smart buildings using audio-processing techniques," in International Conference on Computing in Civil and Building Engineering (ICCCBE) 2016, 2016 Fall.

[65] A. Ebadat, G. Bottega, D. Varagnolo, B. Wahlberg, H. Hjalmarsson, and K. H. Johansson, "Blind identification strategies for room occupancy estimation," in 2015 European Control Conference (ECC), pp. 1315–1320, 2015.

[66] T. Mckenzie and S. J. Schlecht, "Source position interpolation of spatial room impulse responses," Journal of the audio engineering society, May 2023.

[67] A. Sorokowska, P. Sorokowski, P. Hilpert, and K. C. et al., "Preferred interpersonal distances: A global comparison," Journal of Cross-Cultural Psychology, vol. 48, no. 4, pp. 577–592, 2017.

[68] ISO 9613:2024, Acoustics - Attenuation of sound during propagation outdoors - Part 2: Engineering method for the prediction of sound pressure levels outdoors. International Organization for Standardization, 2024.

[69] ISO 9613:1993, Acoustics — Attenuation of sound during propagation outdoors - Part 1: Calculation of the absorption of sound by the atmosphere. International Organization for Standardization, 1993.

[70] A. Weisser and J. M. Buchholz, "Conversational speech levels and signal-to-noise ratios in realistic acoustic conditions," The Journal of the Acoustical Society of America, vol. 145, pp. 349–360, 01 2019.

[71] S. Ross, Introduction to Probability Models. Elsevier Science, 2014.

[72] R. Badeau, "Common mathematical framework for stochastic reverberation models," The Journal of the Acoustical Society of America, vol. 145, pp. 2733–2745, 04 2019.

[73] J.-D. Polack, "Playing billiards in the concert hall: The mathematical foundations of geometrical room acoustics," Applied Acoustics, vol. 38, no. 2, pp. 235–244, 1993.

[74] J. Traer and J. H. McDermott, "Statistics of natural reverberation enable perceptual separation of sound and space," Proceedings of the National Academy of Sciences, vol. 113, no. 48, pp. E7856–E7865, 2016.

[75] M. R. Schroeder, "Frequency-Correlation Functions of Frequency Responses in Rooms," The Journal of the Acoustical Society of America, vol. 34, pp. 1819–1823, 12 1962.

[76] I. Szöke, M. Skácel, L. Mošner, J. Paliesek, and J. Černocký, "Building and evaluation of a real room impulse response dataset," IEEE Journal of Selected Topics in Signal Processing, vol. 13, no. 4, pp. 863–876, 2019.

[77] D. T. Murphy and S. Shelley, "OpenAIR: An interactive auralization web resource and database," in Audio Engineering Society Convention 129, Nov 2010.

[78] J. Thiemann, N. Ito, and E. Vincent, "The Diverse Environments Multi-channel Acoustic Noise Database (DEMAND): A database of multichannel environmental noise recordings," Proceedings of Meetings on Acoustics, vol. 19, p. 035081, 05 2013.

[79] V. Panayotov, G. Chen, D. Povey, and S. Khudanpur, "Librispeech: An ASR corpus based on public domain audio books," in 2015 IEEE International Conference on Acoustics, Speech and Signal Processing (ICASSP), pp. 5206–5210, 2015.

[80] P. Srivastava, A. Deleforge, and E. Vincent, "Realistic sources, receivers and walls improve the generalisability of virtually-supervised blind acoustic parameter estimators," in 2022 International Workshop on Acoustic Signal Enhancement (IWAENC), pp. 1–5, 2022.

[81] M. R. Schroeder, "Modulation transfer functions: Definition and measurement," Acta Acustica united with Acustica, vol. 49, no. 3, pp. 179–182, 1981.

[82] A. Gulati, J. Qin, C.-C. Chiu, N. Parmar, Y. Zhang, J. Yu, W. Han, S. Wang, Z. Zhang, Y. Wu, and R. Pang, "Conformer: Convolution-augmented transformer for speech recognition," in INTERSPEECH (H. Meng, B. Xu, and T. F. Zheng, eds.), pp. 5036–5040, ISCA, 2020.

[83] P. Ramachandran, B. Zoph, and Q. V. Le, "Searching for activation functions," in 6th International Conference on Learning Representations, ICLR 2018, Vancouver, BC, Canada, April 30 - May 3, 2018, Workshop Track Proceedings, OpenReview.net, 2018.

[84] Y. Sun, L. Dong, B. Patra, S. Ma, S. Huang, A. Benhaim, V. Chaudhary, X. Song, and F. Wei, "A length-extrapolatable transformer," in Proceedings of the 61st Annual Meeting of the Association for Computational Linguistics (Volume 1: Long Papers) (A. Rogers, J. Boyd-Graber, and N. Okazaki, eds.), (Toronto, Canada), pp. 14590–14604, Association for Computational Linguistics, 2023.

[85] Y. N. Dauphin, A. Fan, M. Auli, and D. Grangier, "Language modeling with gated convolutional networks," in Proceedings of the 34th International Conference on Machine Learning - Volume 70, ICML'17, p. 933–941, JMLR.org, 2017.

[86] J. Su, M. Ahmed, Y. Lu, S. Pan, W. Bo, and Y. Liu, "Roformer: Enhanced transformer with rotary position embedding," Neurocomputing, vol. 568, p. 127063, 2024.

[87] D. Hendrycks and K. Gimpel, "Bridging nonlinearities and stochastic regularizers with gaussian error linear units," in International Conference on Learning Representations, 2017.

[88] P. J. Huber, "A Robust Version of the Probability Ratio Test," Annals of Mathematical Statistics, vol. 36, pp. 1753–1758, 1965.

[89] L. Ciampiconi, A. Elwood, M. Leonardi, A. Mohamed, and A. Rozza, "A survey and taxonomy of loss functions in machine learning," 2023.

[90] L. Liu, H. Jiang, P. He, W. Chen, X. Liu, J. Gao, and J. Han, "On the variance of the adaptive learning rate and beyond," in International Conference on Learning Representations, 2020.

[91] I.-J. Jung and J.-G. Ih, "Distance estimation of a sound source using the multiple intensity vectors," The Journal of the Acoustical Society of America, vol. 148, pp. EL105–EL111, 07 2020.